Spectral electron energy map of electron impact induced emission of nitrogen

J. Blaško, J. Országh, B. Stachová, Š. Matejčík

Department of Experimental Physics, Faculty of Mathematics, Physics and Informatics, Comenius University in Bratislava

Key words: electron impact, emission cross-section, nitrogen, fluorescence

Abstract

The processes of electron impact induced fluorescence of nitrogen were studied in the electron energy range from 6 to 100 eV and in the spectral range from 330 to 1030 nm. Using the new CCD camera Spectral Electron Energy Map of N_2 was obtained. This type of data in such a wide spectral and energy range are published for the first time. The most intensive molecular emission bands were neutral nitrogen First positive system N_2 ($B\ ^3\Pi_g^+$ - $A\ ^3\sum_g^+$) and Second positive system N_2 ($C\ ^3\Pi_u$ – $B\ ^3\Pi_g$), First negative system N_2^+ ($B\ ^2\sum_u^+$ - $X\ ^2\sum_g^+$) and Meinel system N_2^+ ($A\ ^2\Pi_u$ – $X\ ^2\sum_g^+$). The detected lower intensity transitions were Gaydon-Herman singlet system N_2 ($^1\Sigma_u^+$ - $a^1\Pi_g$ / $^1\Pi_u^+$ - $a^1\Pi_g$) and Gaydon-Green system N_2 ($H\ ^3\Phi_u$ – $G\ ^3\Delta_g$). In addition, processes of dissociative excitation and ionization were observed, resulting in the photon emission from the neutral and singly ionised nitrogen atoms. The provided Spectral Electron Energy Map allows extraction of i) electron energy resolved emission spectra of N_2 and determination of the absolute values of excitation-emission cross sections, ii) excitation-emission functions for any of the molecular bands or atomic lines present in the spectra.

Introduction

Electron induced fluorescence (EIF) technique enables exploration of the electronic, vibrational, and rotational states of molecules through the observed emission of photons and identification of neutral products of electron-molecule collisions. Using EIF, we can observe excitation of optically forbidden excited states of molecules, which are not accessible by photon induced fluorescence. Electron-induced processes are significant in several fields: in the industry (plasma, dielectric discharges, laser physics), in the radiation chemistry, in nanotechnology, in the planetary atmospheres (lightning, aurora, processes in the upper atmosphere caused by cosmic radiation) and in the interstellar chemistry (nebulae, stars, comets). EIF can provide data for remote diagnostics of physical environment of atmospheres around extraterrestrial bodies if electron induced processes are present [1]. The electron induced dissociative excitation and subsequent deexcitation (with the simultaneous photon emission) have also been applicated to identify water plumes emanating from Europa [2] and inner coma of 67P/Churyumov-Gerasimenko [3] or thin oxygen atmosphere around Callisto [4]. The influence of electron induced processes in the atmospheres of planets and small bodies was considered irrelevant in the past. However, this assumption was confirmed as incorrect, because forbidden transitions were detected in the spectra which cannot be stimulated by photons [3]. The photoionization of gases is induced by photons from stars in illuminated atmospheres. Throughout the processes low-energy electrons are detached, and they are entering the electron-induced excitation reactions. The kinetic energy of electrons formed by photoionization is typically in the scale between 0 eV and 100 eV. For several applications such as modelling processes in atmospheres or comas it is especially significant to know the emission cross sections for these reactions. Many atmospheres of extra-terrestrial bodies contain nitrogen (N_2). In the solar system, there are 4 bodies where N_2 is the dominant element in atmospheres: Earth, Titan, Triton, and Pluto [5].

Electron impact excitation of nitrogen is commonly observed in electrical discharges and especially in atmospheric pressure discharges [6,7]. Electron

induced processes in nitrogen gas are also used to determine the rotational and vibrational temperatures of neutrals and ions in plasma discharges [8,9]. Huang et al. [8] studied the temperature by optical emission spectroscopy based on first negative system and second positive system overlapped molecular emission optical spectrum. Nitrogen is also used as a working gas for lasers [6,7].

Several papers on electron impact excitation of N_2 have been published in the past. The first consistent set of total cross sections for excitation of the individual electronic triplet states was first reported by Cartwright et al. [7]. The authors in the paper [10] determined differential and integral cross section for the excitation of electronic transitions by electron impact excitation at incident electron energies of 40 and 60 eV. The integral cross-sections for electron impact excitation were also estimated for five different energies by Campbel et al. [11] and for the near-threshold region by Poparic et al. [12]. The electron impact excitation cross-sections were calculated for several transitions by Chung et al. [13] for relatively large energy range 0 – 2000 eV. The excitation cross sections of atomic lines – products of the electron impact dissociative processes were the focus of Filippelli et al. [14]. The authors report cross sections from the threshold to 300 eV for line in the VUV and UV spectral region. The second positive system of nitrogen was measured by Imami et al. [15–18] and later by Fons et al. [6]. The authors measured cross sections from threshold up to 600 eV. They compared relative optical emission cross sections measured using electron beam experiment with the data from measurement in a discharge tube [6]. The integral excitation cross-sections were determined by Malone et al. [19]. In the article [20], Zubek measured only the emission spectrum of $C^3\Pi_u$ transitions in the region 290 – 410 nm and emission cross section of spectral lines in the electron energy range 11 – 17.5 eV. Mangina et al. [21] measured electron impact emission spectrums of N_2 in the range 330 – 1100 nm at the energy of interacting electrons 25eV and 100eV. They also determined the value of emission cross section at these two energies for most spectral lines. They compared the experimental values with theoretical model and with other publications. Several other papers report electron impact excitation of nitrogen as well [22–24]. Review of the electron and photon collisions with nitrogen cross section was given by Itikawa et al. [25]. In 2012, the article on the 2nd positive-system of N_2 [26] published by our group. The spectrum was measured in the range from 280 to 440 nm and the effective cross sections of selected lines in the electron energy range 6 to 40 eV while the photomultiplier was used as a detector. In the present work CCD camera was used, allowing substantial extension of the measurement spectral range, mainly in the red region of the spectrum

The main goal of this paper is to provide complete set of the excitation-emission cross-section data for N_2. Such data are useful to the scientific communities using optical emission spectroscopy as a diagnostic tool and for simulation of radiative processes in complex systems where electron-molecule collisions play an important role, such as electric discharges, nanotechnological applications or astrophysical environments. The databases of excitation-emission processes are often not comprehensive. The cross-section values are often provided only for selected spectral lines or chosen electron energies. In many publications the cross-sections were measured only in the threshold region, or the cross-sections curves were uncalibrated.

In addition, in present paper, the abilities of the modernized experimental system are demonstrated. The main achievement is the ability to measure two-dimensional spectral electron energy map (SEEM) in the range from 330 to 1020 nm and in electron energy range 6 - 100 eV. The calibrated spectra provide the emission cross-section data for the whole range of wavelengths and energies can be obtained.

Experiment

The used experimental apparatus is based on the concept of collision of an electron and a molecular beam at the 90° angle (see scheme in the Figure 1). In detail it was described earlier in [27–29] In short, the experiment works in binary collision conditions which is achieved by sufficiently low gas pressure – background pressure $1x10^{-4}$ mbar during measurement with lowest pressure $1x10^{-9}$ mbar when gas inlet is closed. Trochoidal electron monochromator generates monoenergetic electron beam with energy resolution 300 meV FWHM. The electrons are thermally emitted from a tungsten filament (Agar Scientic A054). Molecular beam is generated by effusive capillary. The photons emitted during the deexcitation of the excited reaction products are guided by simple optical system from the vacuum chamber to the optical monochromator (Oriel Cornerstone 260 Czerny – Turner) with focal length 0.25 m. Photons

are detected by CCD camera (Andor iDUS 420) and by Hamamatsu photomultiplier (PMT) operating in the photon counting mode. Both detectors are thermoelectrically cooled to increase the signal-to-noise ratio. The CCD camera was added to the system lately and this is the first publication with the new detector. It allows to substantially decrease the measurement time for one spectrum and produce data in the form of a SEEM.

The CCD chip resolution is 1024 x 255 pixels with pixel size 26 x 26 μm. The chip is thermoelectrically cooled to -90 °C to reduce background noise. In contrast to the photomultiplier, where only one spectral point can be determined at once, the optical setup with the CCD camera allows to collect photons from 80 nm wide range of the spectrum in one step leading to resolution approximately 0.078 nm/pixel. This also means the CCD measurements are approximately 800 times faster than PMT if the same integration time and usual PMT step 0.1 nm is used. The spectral range of CCD is from 200 to 1100 nm. However, the sensitivity in the spectral regions 200 – 290 nm and 1030 – 1100 nm is too low. Therefore, the experiment was performed in the spectral range 290 to 1030 nm. The data shown in this paper are in the range 330 – 1030 nm, because the apparatus sensitivity function has not been reliably determined in the region 290 to 330 nm.

The calibration of the electron energy was achieved by measurement of the electron energy dependent cross-section of the (0,0) band of N_2 ($C^3\Pi_u$ - $B^3\Pi_g$) at 337 nm [20] and He I ($1s2p\ ^3P^0_{1,2}$ - $1s4d\ ^3D_{1,2,3}$) 447.14 nm emission line. The cross section of the nitrogen transition exhibits a sharp peak at 14.1 eV and the helium transition exhibits a sharp onset at 23.736 eV.

The electron induced emission spectra of nitrogen were determined in the spectral range from 330 to 1030 nm and in the electron energy range from 6 to 100 eV with varying step: 1 eV step for the range 6-30 eV, 2 eV step for the range 30-50 eV and 5 eV step for the range 50-100 eV. The smaller step was chosen for the ranges where the emission cross-section changes with electron energy rapidly. Each spectrum of the SEEM map was created by joining ten 80 nm spectral ranges with 2.5 nm overlap at both ends.

The raw spectral data were processed in several ways. First, the intensity of each spectrum was corrected for the spectral sensitivity of the system. To achieve the correct intensity scale of the spectra the dependence of the emission intensity on electron energy for the (0,0) band of the nitrogen first negative system was determined. Then the intensity scale of the 25 eV spectrum was adjusted so that the area under the (0,0) band of the second positive system (with peak at 337 nm) corresponds to the emission cross-section value given in [21]. The band was chosen as a reference due to its large absolute cross-section value. Finally, the spectra at other electron energies were adjusted so, that their relative intensities correspond to the shape of determined emission cross-section curve. The resulting SEEM can be used to determine emission cross-section of any detected transition by integrating the surface area under the corresponding spectral band at desired electron energy.

As the whole measurement of the SEEM took considerable time, it was necessary to secure the stability of the system including temperature, electron current, gas pressures, etc. To confirm the stability of the system and reliability of the data we have measured the cross-section curve of the strongest nitrogen feature – the (0,0) band of the first negative system at 391 nm using photomultiplier in one scan and compared the shape with the curve extracted from the SEEM. The curve extracted from the map is slightly deviating from the photomultiplier curve. The deviation is up to 10%. This can pose an extra error in absolute cross-section values determined from the map.

Results

The studied nitrogen emission spectra (330-1030 nm) were initiated by the electron impact at different electron energies (6-100 eV) with a variable electron energy step from 1 to 5 eV. As a result, SEEM was obtained in the above-mentioned ranges. The SEEM provides emission spectra of N_2 as function of electron energy, or the excitation-emission functions for any wavelength covered in spectra. Following processes associated with emission of the photons upon electron impact were identified in the N_2:

i) Excitation-emission of N_2
   $e + N_2(X) \rightarrow N_2^*(B) + e \rightarrow N_2(A) + h\nu$
ii) Ionisation associated with excitation-emission of N_2^+
   $e + N_2(X) \rightarrow N_2^+(B) + e \rightarrow N_2^+(A) + h\nu$
iii) Dissociation of N_2 associated with excitation-emission from excited N

$e + N_2(X) \rightarrow N^*(B) + N + e \rightarrow N(A) + N + hv$

iv) Dissociative ionisation N_2 associated with excitation-emission from excited N^+

$e + N_2(X) \rightarrow N^{+*}(B) + N + e \rightarrow N^+(A) + N + hv$

Spectral electron energy map and excitation-emission functions

The overall SEEM of N_2 is shown in Figure S1 (Supplementary information). Its spectral range is from 330 to 1030 nm and electron energy range from 6 eV up to 100 eV. The lower electron energy limit is well below the threshold of any of the detected processes. The spectral intensity values were calibrated to the values of the excitation-emission cross-sections. After this procedure the SEEM was obtained. The emission cross-sections for the individual processes can be determined by integrating the surface area under the corresponding emission feature (band or line) in the spectrum collected at desired electron energy. The table with the data corresponding to SEEM can be found in the Supplementary information (Table S1). The Figures 2a and 2b present SEEM with improved graphical resolution. The SEEM was divided into 2 separate parts with the main emission systems labelled. The main molecular emission bands in the SEEM (Figures 2a, b) are the first positive system N_2 ($B\ ^3\Pi_g^+ - A\ ^3\sum_g^+$) (1PS), second positive system N_2 ($C\ ^3\Pi_u - B\ ^3\Pi_g$) (2PS), first negative system N_2^+ ($B\ ^2\sum_u^+ - X\ ^2\sum_g^+$) (1NS), and the Meinel system N_2^+ ($A\ ^2\Pi_u - X\ ^2\sum_g^+$) (MS). The Figures 2a and b provide an overview of the active photon emission processes (including the atomic emissions) and allow simple comparison of the threshold energies for individual systems as well as within systems.

Emission spectrum of N_2 initiated by impact of electrons with kinetic energy 25 eV

The emission spectrum of N_2 at 25 eV electron energy was extracted from the SEEM to compare it with the one published by Mangina et al. [21]. At this electron energy the emission from the molecular states of N_2 is strong enough so they can be identified in the spectrum (see Figure 3). The spectrum was divided into 3 parts a-c as large differences in the intensity would render fainter spectral features invisible in one figure. The transitions were identified according to the [21] and [30].

The nitrogen first positive system 1PS is a set of vibronic transitions N_2 ($B\ ^3\Pi_g^+ - A\ ^3\sum_g^+$). In the measured emission spectra, the transitions appear at the wavelengths above 520 nm with the (0,0) band slightly outside our experimental range at 1050.83 nm. In the Figure S3 the nitrogen emission spectra at 8 eV, 10 eV and 12 eV are presented. At 8 and 10 eV only 1PS is visible, while at 12 eV the 2PS appears as its threshold is 11 eV.

The second positive system N_2 ($C\ ^3\Pi_u - B\ ^3\Pi_g$) spans between 290 and 450 nm. The most intensive transition is (0,0) at 337.21 nm. Direct excitation from the ground N_2 ($X\ ^1\sum_g^+$) state to the upper N_2 ($C\ ^3\Pi_u$) state is optically forbidden due to singlet-triplet transition [31]. The upper state can be populated by electron impact via the electron-exchange process. With increasing electron kinetic energy, the nitrogen molecule can undergo ionization-excitation processes. At approximately 17 eV the threshold of the Meinel system and N_2^+ ($A\ ^2\Pi_u - X\ ^2\sum_g^+$) appears and the First negative system N_2^+ ($B\ ^2\sum_u^+ - X\ ^2\sum_g^+$) has threshold at approximately 18 eV. In the spectral region from 400 nm up we have detected several atomic and ionic nitrogen lines (N I and N II). See the Table 1 for more detailed assignment of the bands and lines in the spectrum.

Tab. 1. Transitions detected in the studied spectral range with notation according to [21,30]

Label	Particle	Wavelength (nm)	Transition	Label	Particle	Wavelength (nm)	Transition
1	N_2	346.1	G - H Singlet System ($^1\Sigma_u^+ - a^1\Pi_g$ / $^1\Pi_u^+ - a^1\Pi_g$) 0-4 [30]	28	N I	493.3	$2s^22p^2(^3P)3s – 2s^22p^2(^3P)4p\ ^2P–^2S^\circ$
2	N_2	528.0-530.8	G – G system 1-0 & 2-1 ($H\ ^3\Phi_u – G\ ^3\Delta_g$) [30]	29	N II	500.4, 500.7	$2s^22p(^2P^0)3p – 2s^22p(^2P^0)3d\ ^3D-^3F^0$
3	N_2	537	1st PS ($B\ ^3\Pi - A\ ^3\Sigma$) 12-7	30	N II	553.4, 554.3	$2s2p^2(^4P)3s – 2s2p^2(^4P)3p\ ^5P–^5D^\circ$
4	N_2	540.7	1st PS ($B\ ^3\Pi - A\ ^3\Sigma$) 11-6	31	N I	556.0	$2s^22p^2(^3P)3p – 2s^22p^2(^3P)5d\ ^4D^\circ–^4F$

5	N_2	544.2 547.8	1st PS (B $^3\Pi$ - A $^3\Sigma$) 10-5 1st PS (B $^3\Pi$ - A $^3\Sigma$) 9-4	32	N I	556.4	$2s^22p^2(^3P)3p$ – $2s^22p^2(^3P)5d\ ^4D^\circ$–$^4F$
6	N_2	551.5 555.9	1st PS (B $^3\Pi$ - A $^3\Sigma$) 8-3 1st PS (B $^3\Pi$ - A $^3\Sigma$) 7-2	33	N II	566.6	$2s^22p(^2P^\circ)3s$ – $2s^22p(^2P^\circ)3p\ ^3P^\circ$–$^3D$
7	N_2	559.3	1st PS (B $^3\Pi$ - A $^3\Sigma$) 6-1	34	N II	568.0	$2s^22p(^2P^\circ)3s$ – $2s^22p(^2P^\circ)3p\ ^3P^\circ$–$^3D$
8	N I N II	648.1- 648.6 648.2	$2s^22p^2(^3P)3p$– $2s^22p^2(^3P)4d$ $^4D^\circ$–^4F $2s^22p3s$ – $2s^22p3p\ ^1P^\circ$–^1P	35	N II	568.5	$2s^22p(^2P^\circ)3s$ – $2s^22p(^2P^\circ)3p\ ^3P^\circ$–$^3D$
9	N I	662.9- 663.8	$2s^22p^2(^3P)3p$ – $2s^22p^2(^3P)5s\ ^4D^\circ$–$^4P$	36	N II	571.1	$2s^22p(^2P^\circ)3s$ – $2s^22p(^2P^\circ)3p\ ^3P^\circ$–$^3D$
10	N I	671.2	$2s^22p^2(^3P)3p$ – $2s^22p^2(^3P)4d\ ^4P^\circ$–$^4D$	37	N II	574.8	$2s^22p(^2P^\circ)3s$ – $2s^22p(^2P^\circ)3p\ ^1P^\circ$–$^3D$
11	N I	817.0	$2s^22p^2(^1D)3s$ – $2s^22p^2(^3P)5p\ ^2D$–$^2D^\circ$	38	N I	742.5	$2s^22p^2(^3P)3s$ – $2s^22p^2(^3P)3p\ ^4P$–$^4S^\circ$
12	N I	818.9	$2s^22p^2(^3P)3s$ – $2s^22p^2(^3P)3p\ ^4P$–$^4P^\circ$	39	N I	744.3	$2s^22p^2(^3P)3s$ – $2s^22p^2(^3P)3p\ ^4P$–$^4S^\circ$
13	N I	819.1	$2s^22p^2(^3P)3s$ – $2s^22p^2(^3P)3p\ ^4P$–$^4P^\circ$	40	N I	746.9	$2s^22p^2(^3P)3s$ – $2s^22p^2(^3P)3p\ ^4P$–$^4S^\circ$
14	N I	820.4	$2s^22p^2(^3P)3s$ – $2s^22p^2(^3P)3p\ ^4P$–$^4P^\circ$	41	N I	857.0 859.7 863.2	$2s^22p^2(^3P)3s$ – $2s^22p^2(^3P)3p\ ^2P$–$^2P^\circ$
15	N I	821.4	$2s^22p^2(^3P)3s$ – $2s^22p^2(^3P)3p\ ^4P$–$^4P^\circ$	42	N I	865.9 867.0	$2s^22p^2(^1D)3s$ – $2s^22p^2(^3P)5p\ ^2D$–$^2P^\circ$
16	N I	821.9	$2s^22p^2(^3P)3s$ – $2s^22p^2(^3P)3p\ ^4P$–$^4P^\circ$	43	N I	868.3	$2s^22p^2(^3P)3s$– $2s^22p^2(^3P)3p\ ^4P$–$^4D^\circ$
17	N I	822.6	$2s^22p^2(^3P)3s$ – $2s^22p^2(^3P)3p\ ^4P$–$^4P^\circ$	44	N I	870.6	$2s^22p^2(^3P)3s$– $2s^22p^2(^3P)3p\ ^4P$–$^4D^\circ$
18	N I	824.5	$2s^22p^2(^3P)3s$ – $2s^22p^2(^3P)3p\ ^4P$–$^4P^\circ$	45	N I	871.5	$2s^22p^2(^3P)3s$– $2s^22p^2(^3P)3p\ ^4P$–$^4D^\circ$
19	N I	859.6	$2s^22p^2(^3P)3s$ – $2s^22p^2(^3P)3p\ ^2P$–$^2P^\circ$	46	N I	872.2	$2s^22p^2(^3P)3s$– $2s^22p^2(^3P)3p\ ^4P$–$^4D^\circ$
20	N I	863.2	$2s^22p^2(^3P)3s$ – $2s^22p^2(^3P)3p\ ^2P$–$^2P^\circ$	47	N I	873.2	$2s^22p^2(^3P)3s$– $2s^22p^2(^3P)3p\ ^4P$–$^4D^\circ$
21	N I	868.4	$2s^22p^2(^3P)3s$–$2s^22p^2(^3P)3p$ ^4P–$^4D^\circ$	48	N I	875.0	$2s^22p^2(^3P)3s$– $2s^22p^2(^3P)3p\ ^4P$–$^4D^\circ$
22	N I	904.7	$2s^22p^2(^1D)3s$ – $2s^22p^2(^1D)3p\ ^2D$–$^2F^\circ$	49	N I	903.0	$2s^22p^2(^3P)3p$ – $2s^22p^2(^3P)3d\ ^2S^\circ$–$^2P$
23	N I	938.9	$2s^22p^2(^3P)3s$ – $2s^22p^2(^3P)3p\ ^2P$–$^2D^\circ$	50	N I	906.2	$2s^22p^2(^3P)3p$ – $2s^22p^2(^3P)3d\ ^2S^\circ$–$^2P$
24	N I	939.5	$2s^22p^2(^3P)3s$ – $2s^22p^2(^3P)3p\ ^2P$–$^2D^\circ$	51	N I	982.6	$2s^22p^2(^3P)3p$ – $2s^22p^2(^3P)3d\ ^4D^\circ$–$^4D$
25	N II	404.2	$3p\ ^1S$ – $3d\ ^3P^\circ$ /$3p\ ^1S$ – $3d$ $^3D^\circ$	52	N I	986.6	$2s^22p^2(^3P)3p$ – $2s^22p^2(^3P)3d\ ^4D^\circ$–$^4D$
26	N I	410.0, 410.9	$2s^22p^2(^3P)3s$ – $2s^22p^2(^1D)3p\ ^2P$–$^2D^\circ$	53	N I	1010.6- 1011.7	$2s^22p^2(^3P)3p$ – $2s^22p^2(^3P)3d\ ^4D^\circ$–$^4F$
27	N I	491.3	$2s^22p^2(^3P)3s$ – $2s^22p^2(^3P)4p\ ^2P$–$^2S^\circ$				

Excitation-emission initiated by electron impact of N_2

With this process we associated two emission bands of N_2, the 1st Positive system N_2 (B $^3\Pi_g{}^+$ - A $^3\sum_g{}^+$) and 2nd Positive system N_2 (C $^3\Pi_u$ - B $^3\Pi_g$).

The threshold energy for 1PS has the lowest value of all emission bands detected, starting at approximately 8 eV. The excitation-emission function (EF) (dependence of intensity on incident electron energy) shows sharp increase with electron energy after the threshold and exhibit two maxima at approximately ~10 and ~14 eV after which then significantly decreases to relatively low values (Figure 4a). In Figure 4a the selected series of 1PS excitation-emission functions have the difference in vibrational level of upper and lower state $\Delta v = 2$. In the spectrum these bands can be found between 700 nm and 780 nm. With the increasing upper vibrational level, the threshold energy increases which is even more clearly visible in the SEEM shown in the figure 2b. The above

mentioned two peaks are visible in all EFs in the Figure 4a. According to Stanton et al. [23] the second peak is most probably associated with the cascading radiation from the 2PS N_2. The (6-4) EF increases at electron energies above 20 eV as it is affected by the MS (5-2) transition. Many of the 1PS spectral bands are in the close proximity of Meinel system bands and are blended at energies above 20 eV with the emission from them [23].

The excitation-emission functions for the 2PS exhibits the threshold energy approximately at 10 eV (Figure 4b). Due to 1 eV step in the electron energy, more precise determination of the threshold energies is not possible, but the value is in agreement with more precise studies [17,20,26,31] reporting 11 eV threshold. The EF of the 2PS has a very characteristic shape reaching relatively steep maximum at approximately 14-15 eV, depending on the specific vibrational transition. The transition (0,0) shows the maximum at 14.1 eV [17,20,26,31] Due to this distinctive shape, we have used the curve measurement as one of the two procedures for electron energy calibration as described in the experiment section. As an example, we have selected 2PS EFs for the series with the vibrational level difference between upper and lower state $\Delta v = -2$ (Figure 4b). In the spectrum these transitions appear between 365 nm and 380 nm.

Ionisation associated with excitation-emission initiated by electron impact of N_2

The emission of the photons from excited N_2^+ ions is associated with two emission bands, the Meinel System N_2^+ ($A\ ^2\Pi_u$ - $X\ ^2\sum_g^+$) (MS) and 1st Negative system N_2^+ ($B\ ^2\sum_u^+$ - $X\ ^2\sum_g^+$). The apparent thresholds for the excitation and emission of the N_2 ion MS (~17 eV) and 1NS (~18 eV) are significantly higher compared to 1PS and 2PS. In MS and 1NS sharp peaks close to the thresholds are missing, the EFs of these two systems have broad maxima between 50-100 eV without so significant decrease at higher energies (Figures 4c and 4d). The shown shapes agree with the shapes determined in earlier studies [23,32]. In the present experiment, the electron energy step in the threshold region was 1 eV, the determination of the threshold values bear error up to ±1 eV. However, all present threshold energies are in good agreement with the nitrogen molecule energy levels within the measurement error [33]. The Figure 4c shows a series of 1NS emission functions for emissions from the same vibrational level which exhibit the same threshold. The EFs corresponding to the selected series of transitions of the Meinel system are shown in the Figure 4d.

Weak molecular N_2 bands, dissociative excitation-emission, dissociative ionisation excitation and emission processes of N_2

Apart from the most intensive molecular bands, two very weak bands Gaydon-Herman Singlet system N_2 ($^1\Sigma_u^+$ - $a^1\Pi_g$ / $^1\Pi_u^+$ - $a^1\Pi_g$) (GH) and Gaydon-Green N_2 ($H\ ^3\Phi_u$ – $G\ ^3\Delta_g$) (GG) were detected. In addition to molecular bands, large number of atomic and ionic lines (N I and N II) was detected, corresponding to the dissociative excitation and ionisation processes (see Table 1). The cross-section curves gained from the SEEM for the GG and GH systems are shown in Figure 5. The apparent thresholds for both systems are at approximately 20 eV.

The atomic EFs for N I show two distinctive thresholds at 22 eV and 40 eV (see Figure 6). At the energies below the first 22 eV threshold of both N I EFs there is apparent 1PS EF. In the spectral region between 860 and 875 nm the 1PS (2-1) band is present. The selected EFs for ionised N II with one threshold above 50 eV are shown in the Figure 7. The second threshold would be at energies above the range of our experimental setup. In contrast to other processes the N II EFs continues to rise up to 100 eV.

The emission of the nitrogen atomic cation N II at 500.36 nm represents dissociative ionisation process ($2s^22p(^2P^0)3p$ – $2s^22p(^2P^0)3d\ ^3D$-$^3F^0$), which is blended at lower electron energies (from 20 to 50 eV) with an emission from another process. Based on the EF shape it is most probably the Gaydon-Green emission band. In the Figure S2 the EF taken 499.62 nm at is subtracted from the from the EF at 500.36 nm (corresponding to the N II transition). The shape of the EF at 499.62 nm is the same as the shape of the GG system at 529.23 nm. The match of the EF shapes at 499.62 nm and GG EF at 529.23 nm suggest that GG system extends to the 499.62 nm even though it has not been reported at such wavelengths [30]. After subtraction of the Gaydon-Green EF from the signal at 500.36 nm clean N II EF was obtained with a threshold at approximately 55±5 eV.

Excitation-emission cross-section values and comparison to the earlier published values

The cross-section values of selected transitions were determined by integration of the area under a transition (atomic line or molecular band) in the 25 eV and 100 eV. These cross sections were compared with earlier published values. The present values and their comparison with values of other authors are shown in the Table 2. There is relatively good agreement in the data for most transitions. In the case of the first positive system (1,0) and Meinel system (1,0) transition there is slightly larger discrepancy between our values and values published in [21]. Unfortunately, there are no other publications reporting these cross-sections for comparison. Another source of uncertainty in the comparison is that the authors of cited papers do not provide information on the integration spectral range for each value.

Conclusions

The authors provide full SEEM for the electron impact excitation and emission processes to N_2 as supporting data to this paper. Using the data, scientists may extract calibrated emission spectra of N_2 (330-1030 nm) at any electron energy in the range from 6 to 100 eV. These data also allow extraction of the excitation-emission functions for the processes in this range of electron energies for any N I or N II lines, as well as for any molecular bands of the N_2 and N_2^+. The data may be also used for determination of the excitation-emission cross sections for these electron processes after integration of the surface area under the corresponding atomic lines, or molecular bands. The method for this procedure is described in the paper.

Tab. 2. Selected emission cross-section values at 25 eV and 100 eV electron energy and their comparison with previously published data. The values are shown in $x10^{-18}$ cm^2

Transition	CS value at 25 eV 100 eV	Mangina et al. [21]	McConkey et al. [24]	Stanton et al. [23]	Burns et al. [22]	Fons et al. [6]
1PS (1,0)	6.15 2.2	8.87 1.15		2.32 --		
2PS (0,0)	2.81 0.54	2.81 0.211			3.3 1.097	3.0 0.254
1NS (0,0)	3.15 16.76	2.88 14.9	2.9 15			
1NS (0,1)	1.32 6.27	1.2 5.88	0.928 4.8			
MS (1,0)	4.35 12.2	3.32 8.46				

Acknowledgments

This paper is dedicated to the scientific achievements of Professor Kurt Becker, on the occasion of his 70th birthday.

This work has received support from Slovak Research and Development Agency under the projects nr. APVV-19-0386 and APVV-15-0580, Slovak grant agency VEGA under projects nr. 1/0489/21 and 1/0553/22. This project has received funding from the European Union's Horizon 2020 research and innovation programme under grant agreement No 871149.

References

1. L. Roth, N. Ivchenko, G. R. Gladstone, J. Saur, D. Grodent, B. Bonfond, P. M. Molyneux, and K. D. Retherford, Nat Astron **5**, 1043 (2021).

2. L. Roth, J. Saur, K. D. Retherford, D. F. Strobel, P. D. Feldman, M. A. McGrath, and F. Nimmo, Science (1979) **343**, 171 (2014).

3. D. Bodewits, L. M. Lara, M. F. A'Hearn, F. la Forgia, A. Gicquel, G. Kovacs, J. Knollenberg, M. Lazzarin, Z.-Y. Lin, X. Shi, C. Snodgrass, C. Tubiana, H. Sierks, C. Barbieri, P. L. Lamy, R. Rodrigo, D. Koschny, H. Rickman, H. U. Keller, M. A. Barucci, J.-L. Bertaux, I. Bertini, S. Boudreault, G. Cremonese, V. da Deppo, B. Davidsson, S. Debei, M. de Cecco, S. Fornasier, M. Fulle, O. Groussin, P. J. Gutiérrez, C. Güttler, S. F. Hviid, W.-H. Ip, L. Jorda, J.-R. Kramm, E. Kührt, M. Küppers, J. J. López-Moreno, F. Marzari, G. Naletto, N. Oklay, N. Thomas, I. Toth, and J.-B. Vincent, Astron J **152**, 130 (2016).

4. N. J. Cunningham, J. R. Spencer, P. D. Feldman, D. F. Strobel, K. France, and S. N. Osterman, Icarus **254**, 178 (2015).

5. M. Scherf, H. Lammer, N. v. Erkaev, K. E. Mandt, S. E. Thaller, and B. Marty, Space Sci Rev **216**, (2020).

6. J. T. Fons, R. S. Schappe, and C. C. Lin, Phys Rev A (Coll Park) **53**, 2239 (1996).

7. D. C. Cartwright, Phys Rev A (Coll Park) **2**, 1331 (1970).

8. X.-J. Huang, Y. Xin, L. Yang, Q.-H. Yuan, and Z.-Y. Ning, Phys Plasmas **15**, 113504 (2008).

9. V. Linss, Spectrochim Acta Part B At Spectrosc **60**, 253 (2005).

10. A. Chutjian, D. C. Cartwright, and S. Trajmar, Phys Rev A (Coll Park) **16**, 1052 (1977).

11. L. Campbell, M. J. Brunger, A. M. Nolan, L. J. Kelly, A. B. Wedding, J. Harrison, P. J. O. Teubner, D. C. Cartwright, and B. McLaughlin, Journal of Physics B: Atomic, Molecular and Optical Physics **34**, 1185 (2001).

12. G. Poparić, M. Vićić, and D. S. Belić, Phys Rev A (Coll Park) **60**, 4542 (1999).

13. S. Chung and C. C. Lin, Phys Rev A (Coll Park) **6**, 988 (1972).

14. A. R. Filippelli, F. A. Sharpton, C. C. Lin, and R. E. Murphy, J Chem Phys **76**, 3597 (1982).

15. M. Imami and W. L. Borst, J Chem Phys **61**, 1115 (1974).

16. M. Shaw and J. Campos, J Quant Spectrosc Radiat Transf **30**, 73 (1983).

17. T. G. Finn, J. F. M. Aarts, and J. P. Doering, J Chem Phys **56**, 5632 (1972).

18. Y. Tohyama and T. Nagata, J Physical Soc Japan **80**, 034304 (2011).

19. C. P. Malone, P. v Johnson, J. A. Young, X. Liu, B. Ajdari, M. A. Khakoo, and I. Kanik, Journal of Physics B: Atomic, Molecular and Optical Physics **42**, 225202 (2009).

20. M. Zubek, Journal of Physics B: Atomic, Molecular and Optical Physics **27**, 573 (1994).

21. R. S. Mangina, J. M. Ajello, R. A. West, and D. Dziczek, Astrophysical Journal, Supplement Series **196**, (2011).

22. D. J. Burns, F. R. Simpson, and J. W. McConkey, Journal of Physics B: Atomic and Molecular Physics **2**, 309 (1969).

23. P. N. Stanton and R. M. st. John, J Opt Soc Am **59**, 252 (1969).

24. J. W. McConkey and I. D. Latimer, Proceedings of the Physical Society **86**, 463 (1965).

25. Y. Itikawa, M. Hayashi, A. Ichimura, K. Onda, K. Sakimoto, K. Takayanagi, M. Nakamura, H. Nishimura, and T. Takayanagi, J Phys Chem Ref Data **15**, 985 (1986).

26. J. Országh, M. Danko, A. Ribar, and Š. Matejčík, Nucl Instrum Methods Phys Res B **279**, 76 (2012).

27. J. Országh, M. Danko, P. Čechvala, and Š. Matejčík, Astrophys J **841**, 17 (2017).

28. D. Bodewits, J. Országh, J. Noonan, M. Ďurian, and Š. Matejčík, Astrophys J **885**, 167 (2019).

29. M. Danko, J. Orszagh, M. Ďurian, J. Kočišek, M. Daxner, S. Zöttl, J. B. Maljković, J. Fedor, P. Scheier, S. Denifl, and Š. Matejčík, Journal of Physics B: Atomic, Molecular and Optical Physics **46**, 045203 (2013).

30. A. Lofthus and P. H. Krupenie, J Phys Chem Ref Data **6**, 113 (1977).

31. Shemansky D.E., Ajello J.M., and Kanik I., Astrophys J **452**, 472 (1995).

32. M. Shaw and J. Campos, J Quant Spectrosc Radiat Transf **30**, 73 (1983).

33. M. J. Brunger and P. J. O. Teubner, Phys Rev A (Coll Park) **41**, 1413 (1990).

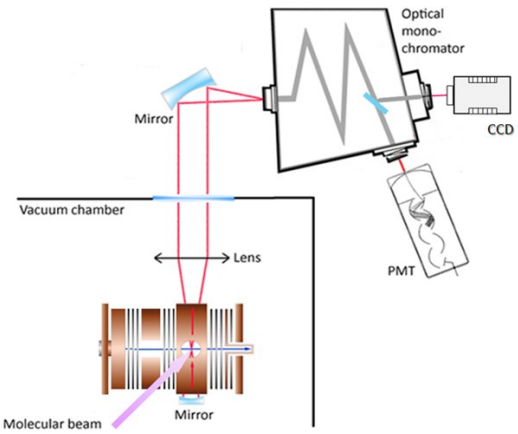

Fig. 1. The scheme of the upgraded electron induced fluorescence apparatus.

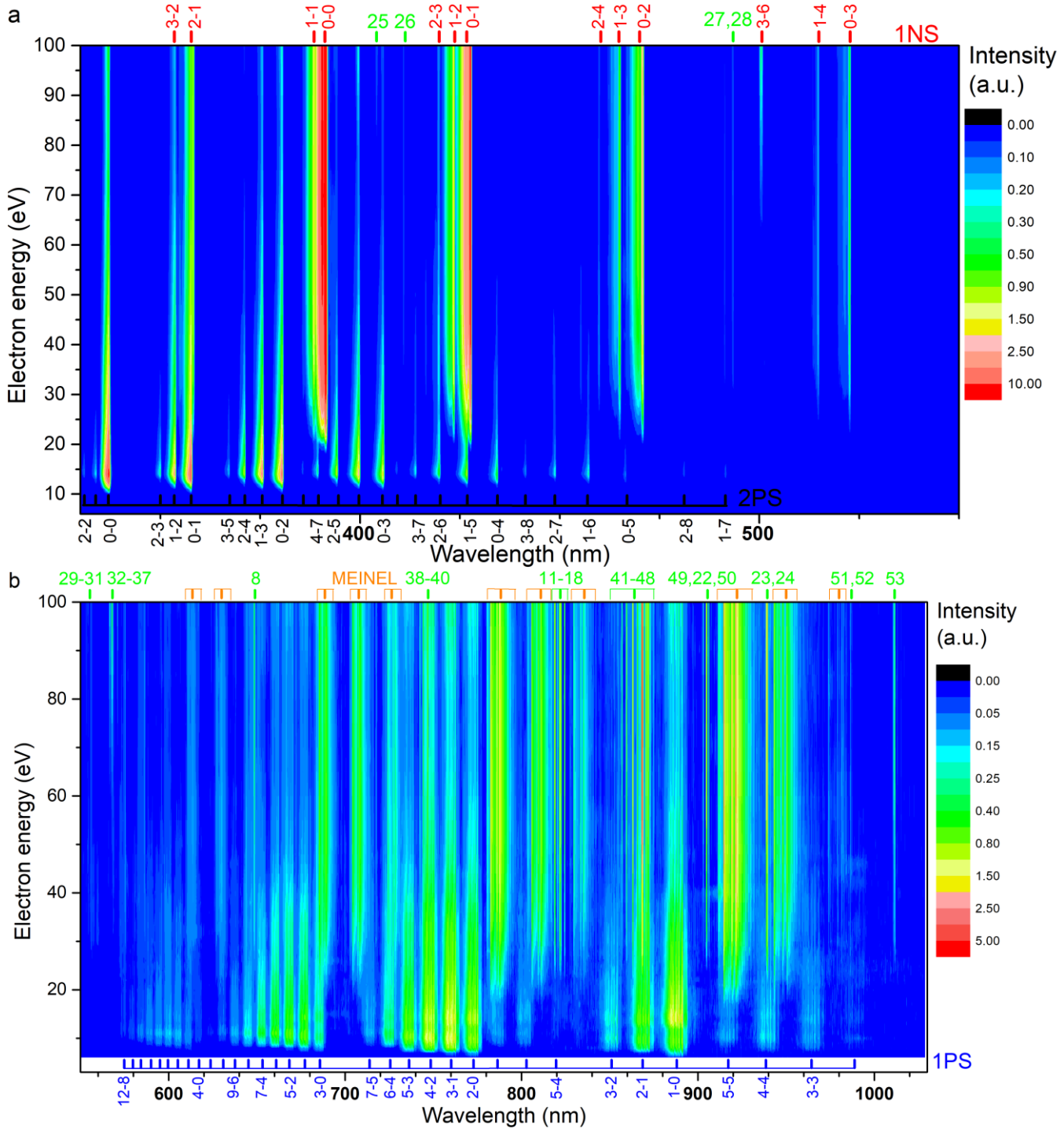

Fig. 2a, 2b. Spectral-cross-section map with main features labelled (for green number labelling see Tab. 1.).

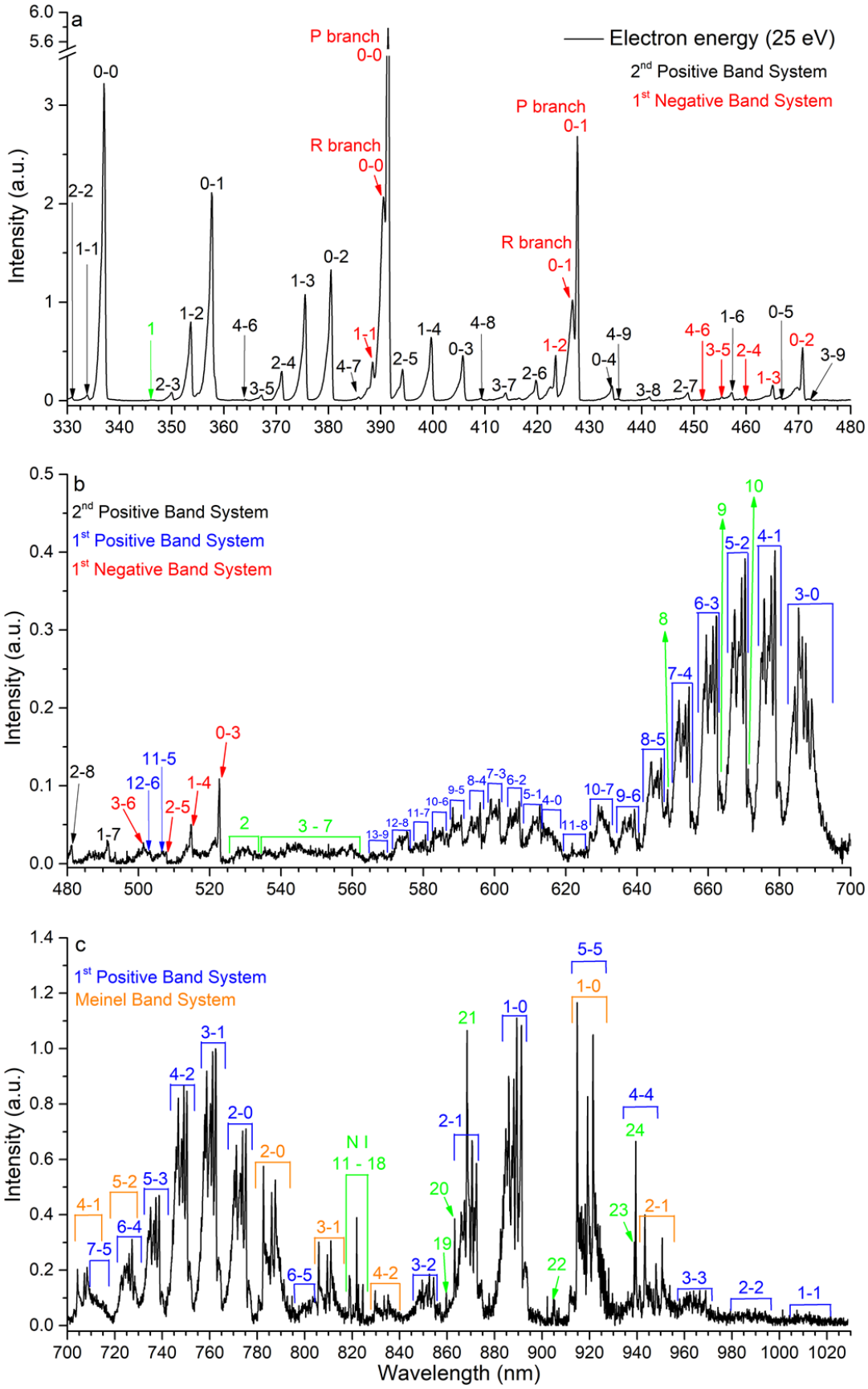

Fig. 3. The emission spectrum of N_2 induced by 25 eV electron impact. The transitions are divided into 4 groups differentiated by colour: blue – 1PS, red – 1NS, black – 2PS, orange – MS with corresponding vibrational transition labelled by numbers in the figures. The green numbers correspond to other transitions listed in Table 1.

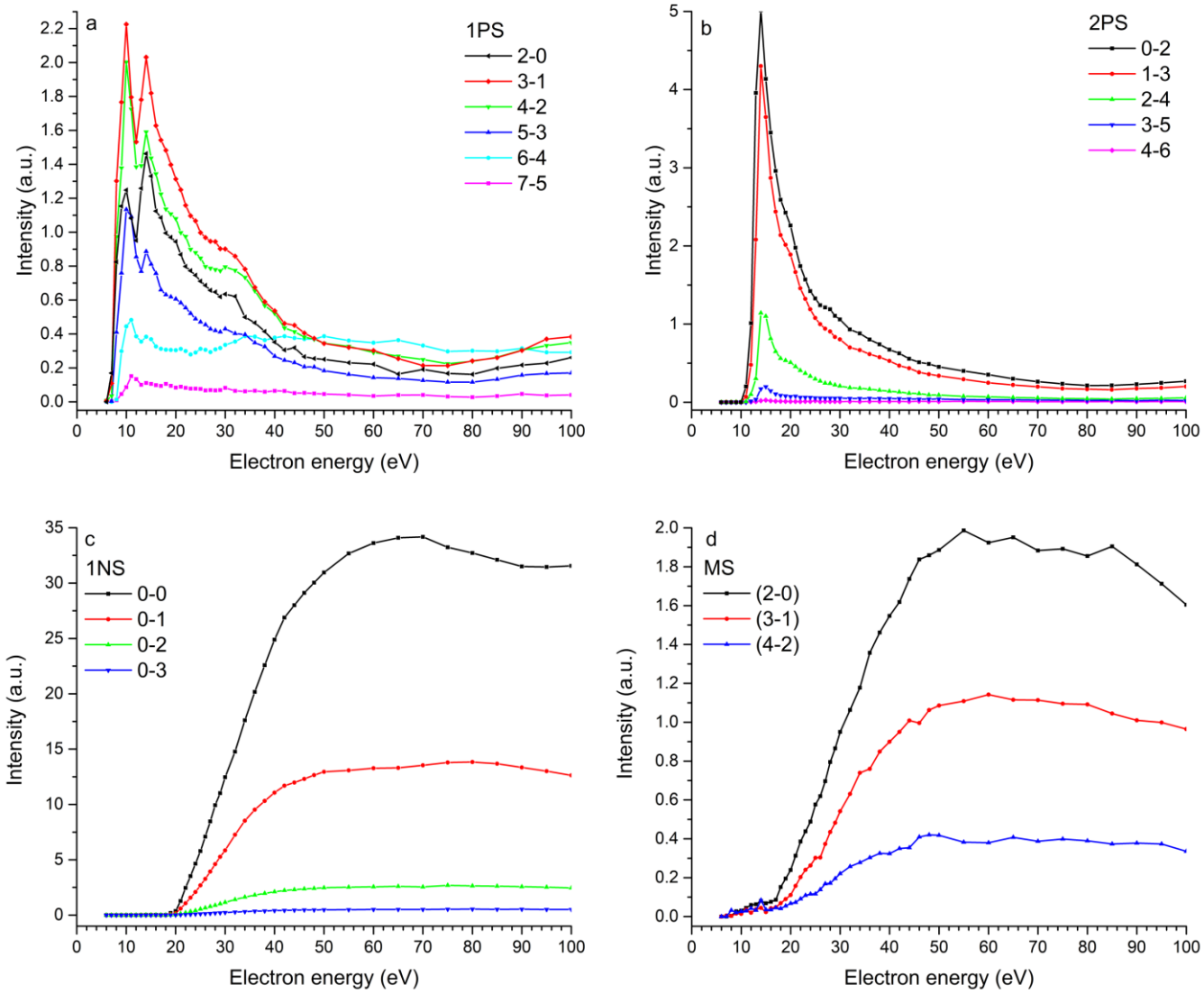

Fig. 4. Comparison of the EFs of the most intensive emission systems of N_2: 1PS EFs with $\Delta v = 2$ (a). 2PS EFs with $\Delta v = -2$ with threshold energies increasing with increasing upper vibrational level (b). 1NS EFs for transitions starting at upper vibrational level zero (c). MS EFs with $\Delta v = 2$ (d).

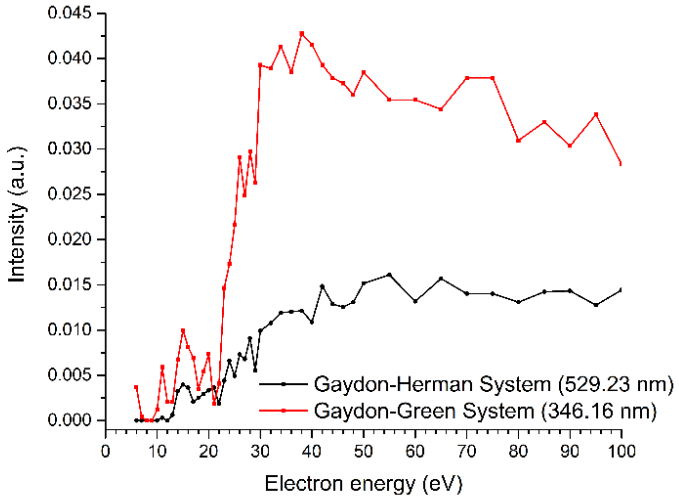

Fig. 5. Excitation-emission functions of the Gaydon-Herman and Gaydon-Green Systems

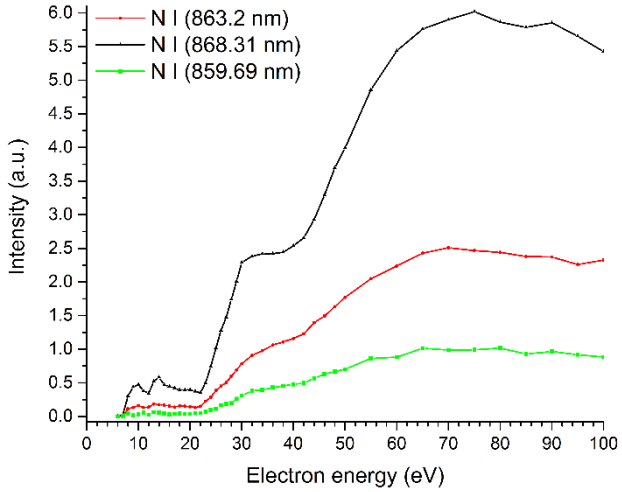

Fig. 6. Excitation-emission functions for selected N I transitions with apparent 1PS EF below the threshold of N I.

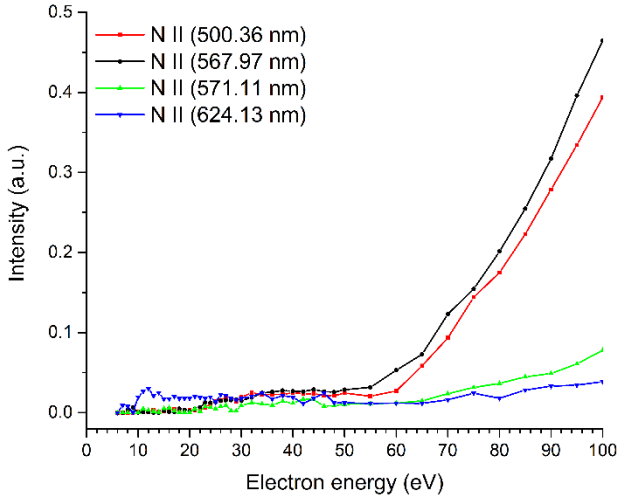

Fig. 7. Excitation-emission functions for selected N II transitions.